Journal of Nuclear Materials 378 (2008) 341–348

Contents lists available at ScienceDirect

Journal of Nuclear Materials

journal homepage: www.elsevier.com/locate/jnucmat

Microstructure and mechanical properties of proton irradiated zirconium carbide

Yong Yang [a,*], Clayton A. Dickerson [b], Hannah Swoboda [b], Brandon Miller [a], Todd R. Allen [a]

[a] Department of Engineering Physics, University of Wisconsin-Madison, Madison, WI 53706, USA
[b] Material Science Program, University of Wisconsin-Madison, Madison, WI 53706, USA

ARTICLE INFO

Article history:
Received 22 January 2008
Accepted 26 June 2008

ABSTRACT

Zirconium carbide is a candidate ceramic being considered for metal-carbide-base composite-type fuels, as well as for an alternative coating material for TRISO particle fuels. Ensuring adequate mechanical properties and dimensional stability in response to radiation is a key part in developing a practical ZrC-base fuel. The existing available radiation response data for ZrC is limited and insufficient. In the present study, ZrC was irradiated with a 2.6 MeV proton beam at 800 °C to doses of 0.7 and 1.5 dpa. Following radiation, the radiation induced damage microstructure is comprised of a high density of nanometer-sized Frank loops, but no irradiation induced amorphization, voids, or precipitates were observed. A slight lattice expansion was found in the irradiated ZrC, in good agreement with the reported results from neutron irradiation. The changes in microhardness and fracture toughness properties induced in the irradiated samples were measured using indentation techniques. The hardness and the fracture toughness both increase with increasing radiation dose.

1. Introduction

ZrC is typical transition metal-carbide that takes the NaCl ground-state crystal structure. Prior to irradiation, ZrC has several exceptional characteristics including hardness, corrosion resistance to fission products, high melting point of ~3540 °C (46.5% carbon atoms), and imperviousness to hydrogen attack [1–3]. Due to a combination of acceptable neutronic performance, thermal properties, chemical behavior, and physical properties, ZrC was selected as one of five alloys with the highest potential for success as a carbide-base composite-type (CERCER) fuels for the gas-cooled fast reactor (GFR) [4]. Additionally, because of a high fission product retention capability, ZrC is one of the most promising alternative materials for the fuel kernel and/or coating system in microencapsulated coated particle fuels for VHTR application [5,6]. Determining and predicting the stability in response to radiation is a key part in developing a practical ZrC-based fuel, but an impediment to this objective includes the cost and time required for neutron irradiation.

The primary irradiation effects of technological importance occurring in ceramics under radiation are dimensional instability, changes in transport properties, and changes in mechanical properties [7]. A limited number of ZrC TRISO-type fuel particles have been irradiated to low burnup, but detailed post-irradiation microstructural analysis of the ZrC layer was not published [5,8–10]. Some ZrC data have been generated under a limited range of irradiation condition [11–14]. These studies show a ZrC lattice parameter increase at a neutron fluence of ~1.5×10^{20} n/cm^2 (0.2 dpa) at 50, 150 and 1100 °C with lattice parameter increase of 0.32%, 0.47% and 0.12%, respectively. The work by Patriarca et al. on ZrC and TiC irradiated in the Engineering Test Reactor (ETR) at temperature of 130–355 °C to a dose of ~7.5 dpa showed a volume increase of ~3% and 2–3% for ZrC and TiC, respectively, [13]. Keilholtz et al. reported the volumetric expansion of ZrC irradiated with fast neutrons at 300–700 °C in the ETR. A ~3% volume increase at a dose of ~3 dpa was measured. The major cause of damage to carbides is postulated to be the accumulated point defects, and less than 50% of the crystal expansion was accounted for by increases in lattice parameters [14]. Recently, Gan et al. used 1 MeV Kr irradiation at 800 °C to study the microstructural stability of ZrC, and found a lattice expansion of approximately 7% for ZrC irradiated to 70 dpa while no radiation induced amorphization was observed [15]. After 4 Mev Au ion irradiation at room temperature, Gosset has also shown a moderate swelling and high internal stress which both saturate at a Au fluence around 10^{14} cm^{-2} corresponding to a few dpa, and there is a high density of small faulted dislocations revealed by TEM [16]. In addition, the properties of ZrC are often sensitive to the stoichiometry [17,18] and the irradiation behavior are very likely related to the C/Zr ratio, as reported by Andrievskii, the sub-stoichiometric materials damaged relatively less than the nearly-stoichiometric ones under the neutron irradiation in a large stoichiometric range [19]. In summary, the limited neutron and heavy ion exposures are insufficient to fully understand the microstructural stability of ZrC under radiation. Additionally, no neutron irradiated microstructures have been identified in the open

* Corresponding author. Tel.: +1 608 2635444; fax: +1 608 2637451.
E-mail address: yyang@cae.wisc.edu (Y. Yang).

0022-3115/$ - see front matter © 2008 Elsevier B.V. All rights reserved.
doi:10.1016/j.jnucmat.2008.06.042

Table 1
Chemical composition of ZrC [15]

Element	Ti	Zr	Si	Hf	Fe	Mo, Pt, Y, W	C	N	O	Other
wt%	0.19	84.8	<0.001	1.91	<0.01	<0.1	11.3	0.61	0.21	<0.01

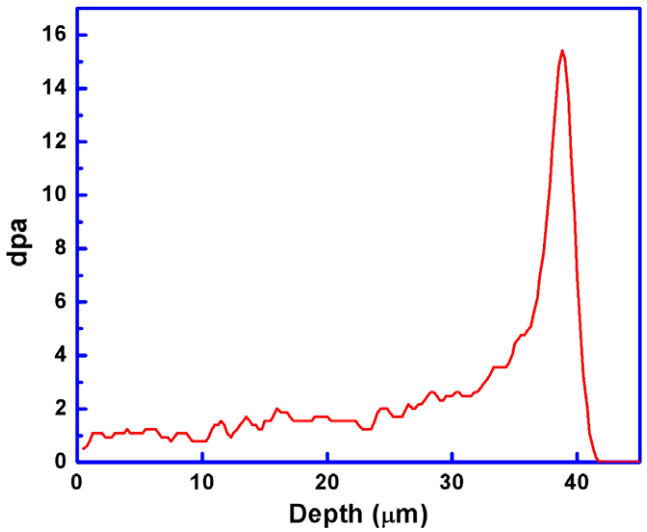

Fig. 1. SRIM estimation of damage in ZrC irradiated with $1 \times 10^{19}/cm^2$ 2.6 MeV protons.

literature. This paper presents the microstructure and mechanical property changes produced by proton irradiation under a temperature of 800 °C.

2. Experiments

Commercial grade ZrC rods were obtained from CERCOM Inc. (Vista, California 92801), the ZrC was produced by vacuum hot pressing of powder which is commercial product from H.C. Stark Inc. (Newton, MA 02461). The ceramic was received as 25 mm long rods with a diameter of 3 mm, and the density was measured as 6.58 g/cm^3. The Idaho National Laboratory (INL) chose this lot of ZrC for the FUTURIX irradiation program and the chemical compositions performed at NSL Analytical Services, Inc. with ICP-MS and Leco methods, are listed in Table 1. The ratio of C/Zr is 1.01 and nearly-stoichiometric. Prior to irradiation, the porosity and the grain size distribution were examined using scanning electron microscopy (SEM).

Irradiation was conducted using a 2.6 MeV proton beam. The damage profile, calculated using TRIM2008 (Transport of Ions in Matter) [20] with the threshold displacement energies of 35 eV for zirconium and 25 eV for carbon based on the estimation from Gosset [16], is shown in Fig. 1. The depth of greatest interest is the 'flat' region 10–30 μm before the peak, and this region is where the dpa was calculated. The damage rates were taken from the 'Full Damage Cascade' calculation condition, and the calculated dose rate is approximate 2×10^{-5} dpa/s. Two irradiation doses of 0.7 dpa and 1.5 dpa were performed on the samples at a temperature of 800 °C measured by the three stage-embedded thermocouples, and the experimental temperature was achieved by heating the sample stage via a Gaumer GB301X-500-CB cartridge heater to a temperature below that which will be reached when the beam was introduced. The irradiation temperature deviations are ±23 °C and ±9 °C for the doses of 0.7 dpa and 1.5 dpa, respectively. To examine the effect of temperature alone, the as-received ZrC was also annealed at 800 °C for 20 h (corresponding to the time required to get to 1.5 dpa) in a vacuum furnace.

The to-be-irradiated ZrC discs were sliced from the ceramic rods using a low speed diamond saw, followed by wet-grinding down to 250 μm thickness and finished with 1 μm diamond paste on both sides. After irradiation, a thin layer of ~10 μm was removed from the irradiated side to eliminate the surface effects from the subsequent microstructural and mechanical property studies. The TEM samples were prepared using wedge polishing followed by low angle ion milling. For the irradiated sample, the electron transparent area was controlled to be at the middle of the radiation damage range, which is about 20 μm deep from the irradiated surface. The TEM characterization was conducted using a JEOL 200CX-II and a Philips CM200UT TEM, and the possible radiation induced segregation across the grain boundaries or the dislocation loops were examined using electron dispersive spectroscopy (EDS) with a spot size of 6 nm diameter. The SEM microstructure of the unirradiated sample was characterized using a FIB Zeiss CrossBeam. To study the lattice expansion caused by proton irradiation, X-ray diffraction (XRD) was conducted using a STOE X-ray Powder Diffractometer. The microhardness and fracture toughness properties were measured using a Micromet 2003 micro indenter, and the sample surfaces were lapped up to 1μm diamond and finished with the ~0.04 μm silica polishing.

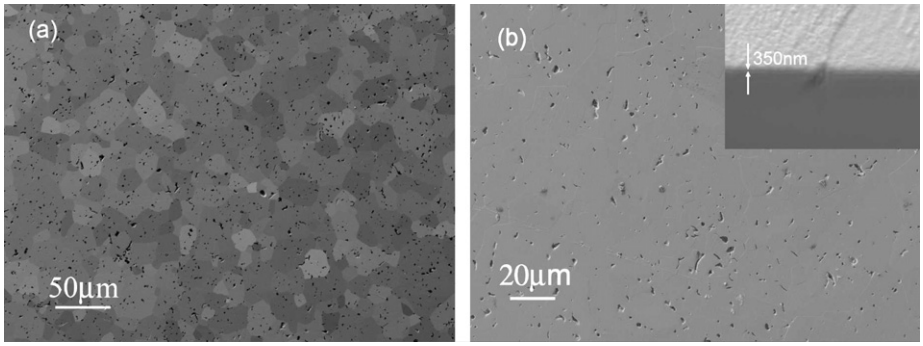

Fig. 2. (a) SEM image of unirradiated ZrC grain structure and (b) SEM image of the sample surface of ZrC after irradiation, FIB image of the cross-section revealing an oxide layer on the irradiated surface.

3. Result and discussion

3.1. Microstructure

3.1.1. SEM

The SEM image in Fig. 2(a) clearly displays the grain structure of the annealed ZrC. The material has relative low porosity, no apparent inclusion phases were identified, and the average grain size is ~24 μm. After irradiation, a thin oxidation layer was found on the irradiated surface but no indication of grain boundary separation in any case as shown in Fig. 2(b). The thickness of the oxidation was measured from the cross-section of the trench ion milled using a focused ion beam milling and it is about 350 nm.

3.1.2. TEM

The possibility of void structures was examined carefully at high magnification under a kinematic condition by means of a through-focus technique. No voids or bubbles were observed in the unirradiated or irradiated samples with the image resolution up to less than 1 nm. However, Gan found some nanometer-sized bubbles in the unirradiated ZrC (Gan analyzed the same ZrC from CERCOM) sample prepared by ion milling [15], and this discrepancy may be due to the different ion milling conditions, for our sample preparation, low angle $\leqslant 9^\circ$, low voltage $\leqslant 4$ kV and very short milling time were used.

Fig. 3 shows the images taken close to a near [011] zone axis under a $g = 200$, 2-beam bright field condition, and images with

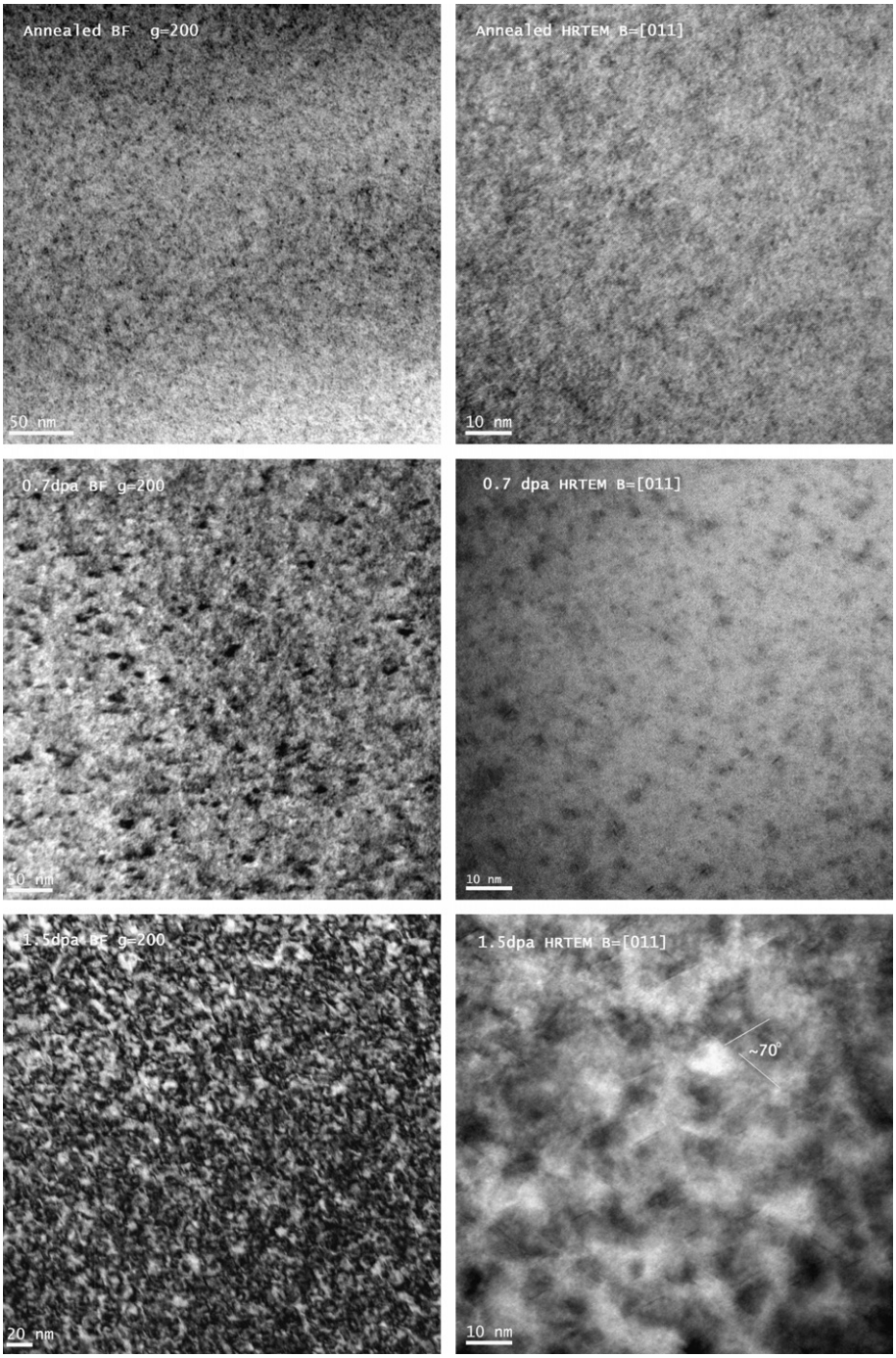

Fig. 3. Bright field and HRTEM images for annealed and irradiated ZrC.

high resolution taken at the [0 1 1] zone axis. The microstructure of the annealed ZrC mainly consists of scattered nanometer-size black spots which were induced by the ion milling during sample preparation. No dislocation lines or precipitates were identified, and the diffraction pattern obtained by titling the sample away from the [0 1 1] zone axis along $g = 3\,1\,\bar{1}$ does not show any rel-rod streaks in the unirradiated ZrC.

Information about the expected damage microstructure of irradiated ZrC can be inferred from the collision cascades, as simulated by Brutzel et al. using molecular dynamics simulation at the temperature of 300 K [21]. In these calculations, no amorphization was observed and all the Zr interstitials form a dumbbell structure oriented in the ⟨1 1 1⟩ direction and C interstitials are either isolated or form a ⟨1 1 1⟩ dumbbell structure. Clusters of interstitials of two different species have a tendency to form interstitial dislocation loops in the {1 1 1} plane. Some isolated vacancies or small vacancy clusters, involving bother C and Zr vacancies, were found in the core of the cascade. In our experimental study, Flank Loops (FLs) in the plane {1 1 1} were observed in the irradiated sample at both dose levels 0.7 and 1.5 dpa. Based on the HRTEM images and DF images, FLs are the only identified defects with observable density in the proton irradiated ZrC. The size and the density of loops increases as the dose level increases, as displayed in the HRTEM images. From the bright field images at the $g = 2\,0\,0$ 2-beam condition, it can be seen that the microstructure of irradiated ZrC matrix becomes highly strained locally as the doses increases. Due to the local lattice distortion, no Kikuchi bands can be observed in the convergent beam diffraction for the sample with dose of 1.5 dpa as shown in Fig. 4. Additional details of the defect structures are shown in lattice plane resolution image, Fig. 5. The near edge-on Frank loops can be identified clearly, while no obvious stacking fault tetrahedron (SFT) was observed.

As one of the major microstructural defects in irradiated samples with an fcc structure, faulted dislocation loops lie on the four {1 1 1} planes with a Burgers vector $a/3$ ⟨1 1 1⟩ and can be clearly delineated in materials using the Rel-rod technique. The relevant diffraction condition was conducted by tilting the sample close to the $g = 3\,1\,\bar{1}$ 2-beam condition near the ⟨0 1 1⟩ zone axis, and the Rel-rod dark field image is formed from the Rel-rod streak selected by the objective aperture. The diffraction conditions are schematically shown in Fig. 6(a). The density of the Frank loops can be determined from this orientation by multiplying by four to account for the three variants not being imaged assuming an isotropic distribution. The measurements were performed near the edge of the wedge samples to minimize the overlap of the defects and improve the accuracy of the results. The size distributions of FLs in the irradiated ZrC are displayed in Fig. 7. For the irradiation to 0.7 dpa, the size distribution of FLs tends to be narrow, but as the dose increases, the distribution broadens and the loops appear to grow, shifting the average size upward. The density of the FLs in the sample with dose of 1.5 dpa is much higher than that of 0.7 dpa, as summarized in Table 2. There is no known published microstructural characterization for neutron irradiated ZrC for comparison. For the Kr irradiated ZrC from Gan et al., no clear Frank loops structures or irradiation induced line dislocations were observed in the sample irradiation up to 70 dpa at 800 °C [15].

Irradiation also led to changes in the near-boundary regions in the form of defect-denuded zones as illustrated in Fig. 8. For each dose level, more than 6 grain boundaries were measured, and for each measurement, the grain boundary plane was tilted to parallel with the electron beam. The measured widths of these zones are summarized in Table 3. As the dose increases, the average width of the denuded zone tends to be narrower. However, the large variation in width may be related to different boundary characters with associated grain boundary energies. According to Eq. (6) in the paper by Zinkle, the measured denuded zone widths at several different irradiation temperatures or damage rates can be used to evaluate the interstitial diffusivity provided that the bulk interstitial concentration over the difference between the bulk interstitial concentration and critical interstitial concentration is relatively independent on the irradiation temperature or dpa rate [22]. This evaluation will be the focus of future studies.

The samples were also examined for possible radiation induced segregation (RIS) using EDS. No detectable elemental depletion or

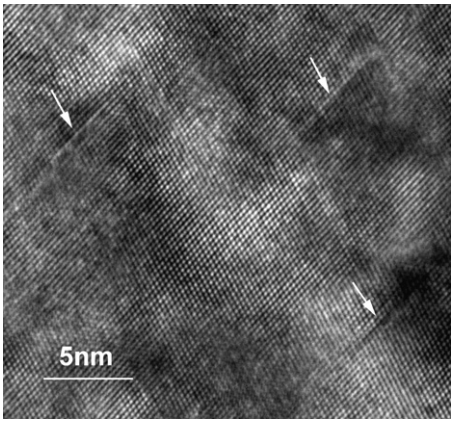

Fig. 5. Lattice resolution image of Frank loops indicated with arrows.

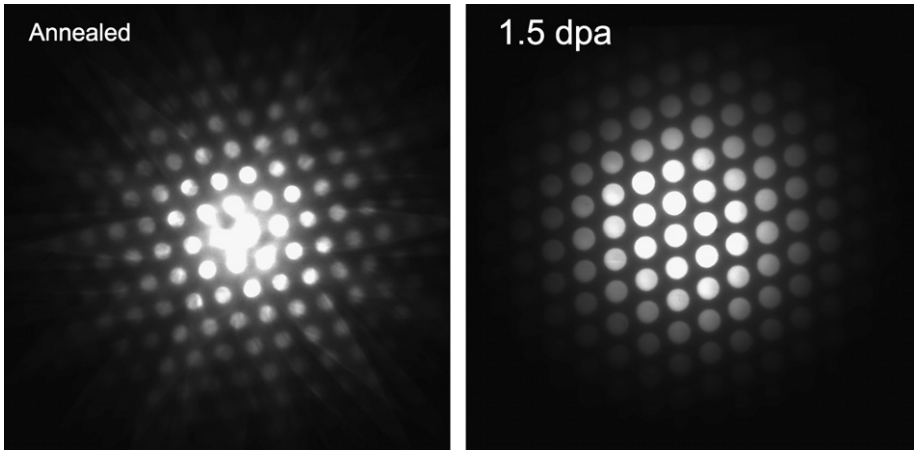

Fig. 4. Convergent beam diffraction patterns on unirradiated and 1.5 dpa irradiated ZrC.

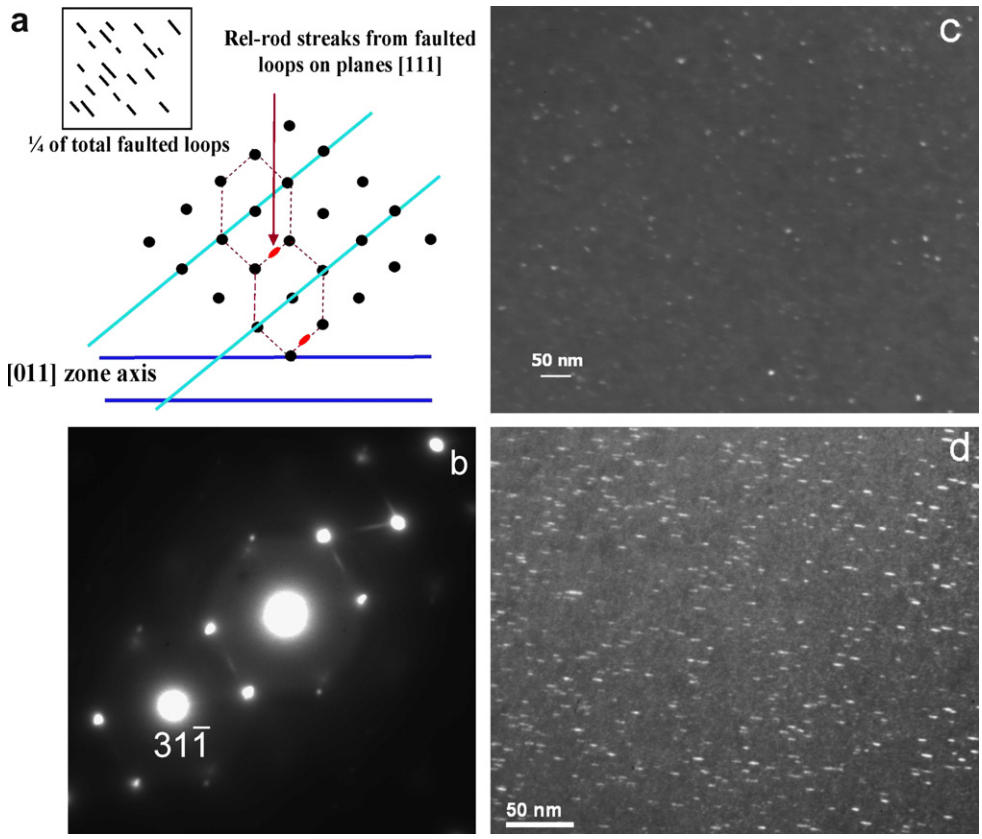

Fig. 6. Rel-rod dark field image of FLs (a) schematic of the diffraction condition, (b) diffraction pattern at $g = 3\,1\,1$ near [0 1 1] zone axis, (c) sample with dose of 0.7 dpa and (d) sample with dose of 1.5 dpa.

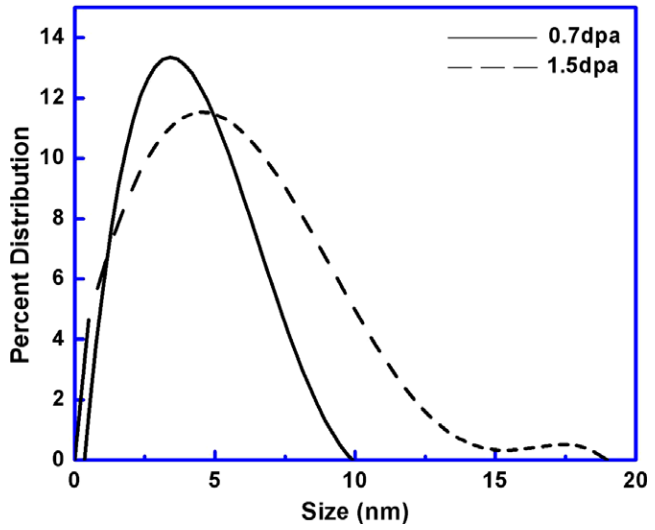

Fig. 7. Frank loop size distributions in irradiated ZrC.

Table 2
Average size and density of Frank loops in the irradiated ZrC

Dose (dpa)	Loop density ($\times 10^{23}$ m^{-3})	Mean size (nm)
0.7	0.22 ± 0.044	4.3 ± 0.524
1.5	3.37 ± 0.123	5.8 ± 0.578

enrichment was found at the GBs in the irradiated ZrC, but due to the limitations of the resolution in the TEM used, segregation cannot be ruled out until measurements are attempted using an appropriate TEM. Similarly, no profiles were successfully obtained across the Frank loops oriented edge-on. RIS will be further studied using Electron Energy Loss Spectroscopy (EELS) in our future research.

3.2. Lattice expansion

XRD scans of ZrC have shown very small peak shifts to lower 2θ values with increasing dose, as displayed in Fig. 9. Guided by Bragg's law, $\lambda = 2d.\sin\theta$, if an observed peak shifts to smaller values of 2θ, an accompanying increase in d, the plane spacing corresponding to a specific set of planes, must occur since the wavelength of the X-rays remains constant. The preliminary analysis of the XRD data has shown lattice parameter differences of less than 0.2%. Because of these very small changes and the possible incorporation of alignment and positioning errors, measures were taken to eliminate the error in the data to obtain more accurate lattice parameters by using alumina as a reference marker. The 2θ of each scan was corrected with the standard peaks of alumina, and the lattice parameters were calculated using the Werner's function in Winxpow® [23].

The increments of the lattice parameter of ZrC at different irradiation doses are displayed in Fig. 10, and the increase in lattice parameter is about 0.11% for the dose of 1.5 dpa and 0.09% for the dose of 0.7 dpa. For the Kr ion irradiated (70 dpa) ZrC, about 7% lattice expansion was reported [15]. While for the fast neutron irradiated samples examined by Keilholtz et al., the X-ray patterns were obscured and the data scattered too much to draw conclusions concerning whether there was an increase or decrease in lattice spacing with increasing neutron dose, even though a 2–3% volume change was observed for ZrC samples irradiated to 3–8 dpa at a temperature of 300–700 °C. Less than 50% of the

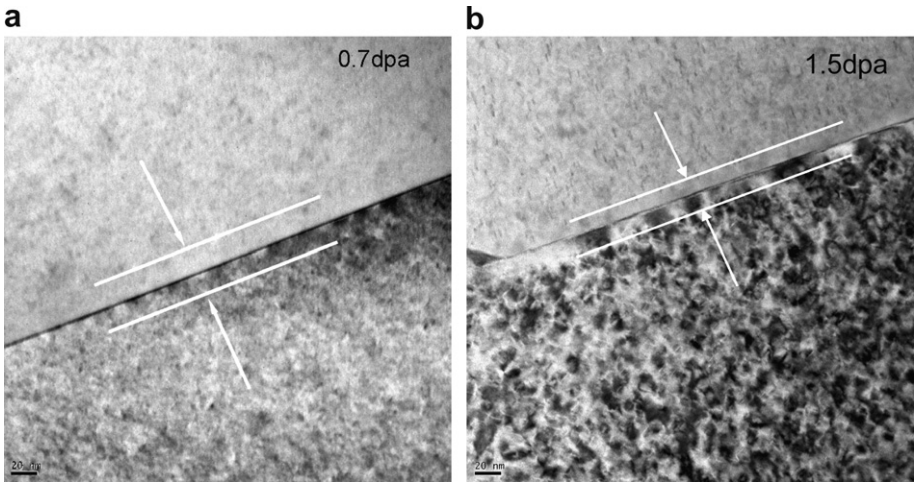

Fig. 8. Denuded zones were found in the irradiated ZrC at a 2-beam $g = 200$ condition.

Table 3
The denuded zones width at GBs in irradiated ZrC

Dose (dpa)	Denuded zone width (nm)
0.7	45.1 ± 6.1
1.5	26.8 ± 4.4

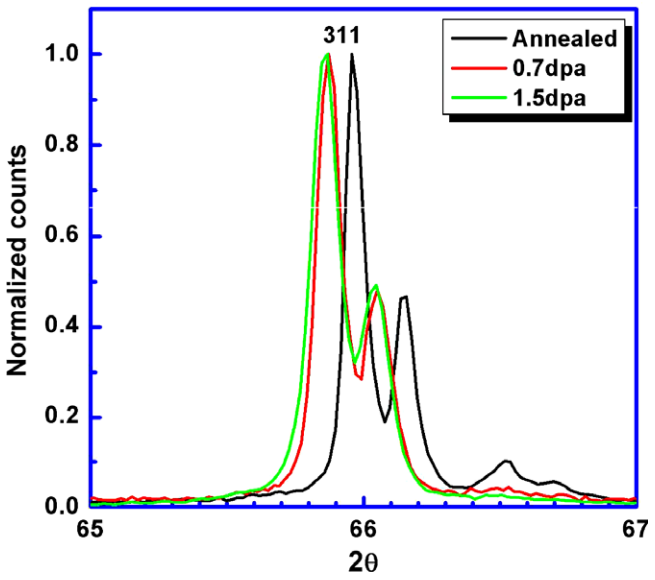

Fig. 9. X-ray diffraction of ZrC with different irradiation doses.

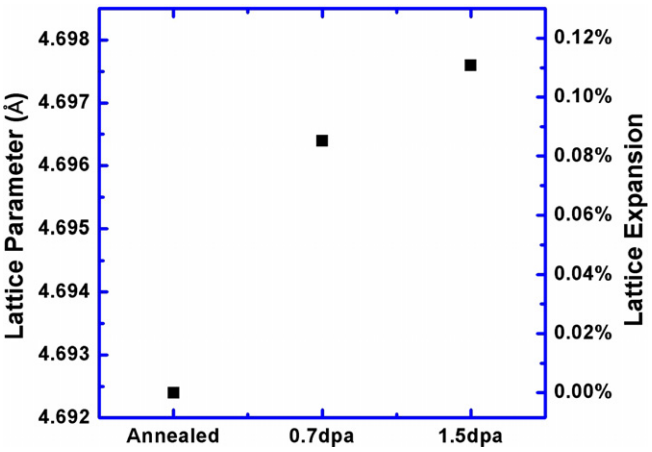

Fig. 10. Lattice parameters and increments of ZrC with different irradiation doses.

crystal expansion was postulated to be from lattice parameter change [14]. For the ZrC irradiated with thermal neutrons at 50 °C, the increase of lattice parameter reached 0.32% at a dose of 1.5×10^{20} cm^{-2} [13], while for samples irradiated at 150 °C and 1100 °C with neutron a dose of 1.5×10^{20} cm^{-2} ($E \geqslant 1$ MeV), the lattice expansions were 0.46% and 0.12%, respectively, [12]. Generally, the lattice expansions in our study are in good agreement with the results from neutron irradiation.

3.3. Mechanical properties

3.3.1. Microhardness

Since a high density of dislocation loops was observed in irradiated ZrC, it is reasonable to study the irradiation hardening. Measurements of annealed and irradiated ZrC were conducted with a Vicker's hardness tester using a 1000 gf load and 15 s load time according to the ASTM standard [24]. Many empirical rules and formulae have been proposed to precisely and reliably measure the mechanical properties of hard thin films. Recalling Fig. 1, the proton irradiated sample is roughly the equivalent of a thin film of different hardness on top of the unirradiated material unaffected by the proton beam. To eliminate the influence of substrate deformation, the upper limit of indentation depth is proposed to be below about 1/5 of the film thickness [25], though the ratio recommended by the ASTM standard is 1/10 [24]. The indention depth with 1000 gf load on ZrC in our study is ~4.5 μm, which is well below the 1/5 of the irradiated zone; while with a load of 500 gf, the indentation depth can be shallower, but the corresponding smaller diagonals of impression can introduce a considerable measurement error. The increase of the microhardness due to irradiation is 12.5% for 0.7 dpa and 14% for 1.5 dpa, as displayed in Fig. 11. The microhardness changes caused by neutron irradiation in ZrC were also measured by Andrievskii et al., for the irradiation dose of 1.5×10^{20} cm^{-2} at 150 °C and 1100 °C. In that work, the increment of hardness in ZrC was 12% and 7%, respectively, [12]. The irradiation caused hardening in ceramics are mainly attributed to the formation of point defects, the strain fields around the point defects can interact with the dislocations during deformation and act as a pinning center, the point defects

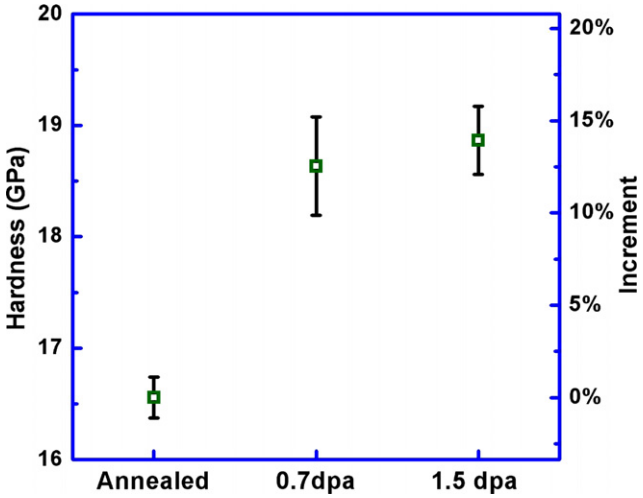

Fig. 11. Microhardness changes in ZrC versus different dose levels.

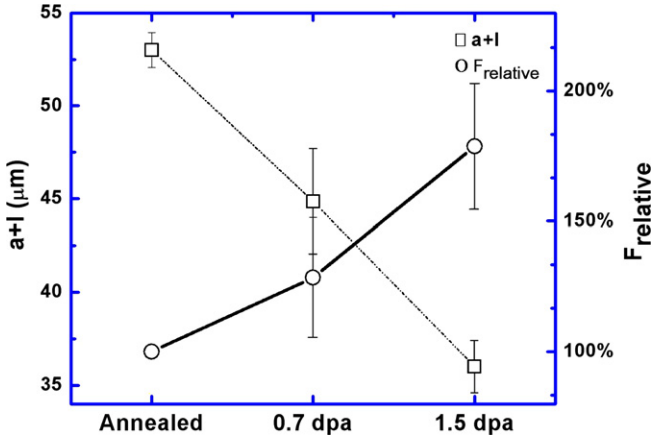

Fig. 13. Fracture toughness changes of the ZrC with different irradiation doses.

can play an important role in dynamic processes such as crack propagation.

3.3.2. Fracture toughness

The change in fracture toughness as a function of irradiation is a critical data need for advanced fuel forms, but with the exception of graphite and very limited information on alumina, magnesium aluminate spinel and silicon carbide, there is very little information on the effect of irradiation on the fracture toughness of ceramics. Due to the irradiation volume limits of proton irradiation, the fracture toughness of ZrC cannot be measured using conventional pre-cracked beam method, instead, it is estimated by measuring the length of cracks produced by hardness indents. For this measurement, Vickers micro-indentation is specifically considered because it uses a sharp indenter that produces well-defined cracks.

The cracks produced by micro-indentation can be divided into two classes, classic median/radial 'half-penny' cracks and 'Palmqvist' cracks. The primary difference between half-penny and Palmqvist crack systems exists in the sub-surface cracking of the material. In the half-penny system, cracks emanate from the indentation tips laterally and radially, and lateral cracks travel along the surface, while the radial cracks protrude from the indention in a starburst within a radius below the surface of the material. In the Palmqvist crack system, cracks only travel laterally. Notice the variables *c*, *l*, and *a* in Fig. 12, the variable *a* indicates half the length of the diagonal of the indent, *l* indicates the length of a crack from the tip of the indent to its termination in the material and the variable *c* is the sum of *a* and *l*. Based on the criterion established in our previous study [26], a *c*/*a* value greater than or equal to 2 indicates a half-penny crack system. For lower *c*/*a* values, a Palmqvist crack system is assumed. For ZrC, based on the *c*/*a* value emanating from indents, a half-penny crack system was assumed and corresponding estimates of the change of fracture toughness were performed, as shown in Fig. 12.

After determining *a, l, c* and the crack system, the relative fracture toughness was calculated according to Eq. (1), which is valid for a half-penny crack system.

$$\frac{K_{IC}}{K_{ICo}} = \frac{c_o^{\frac{3}{2}}}{c^{\frac{3}{2}}} = \frac{(a_o + l_a)^{\frac{3}{2}}}{(a+l)^{\frac{3}{2}}}, \tag{1}$$

where the subscript 'o' denotes the annealed samples.

The values of the relative fracture toughness are plotted in Fig. 13 based on more than 20 measurements for each condition, and the greatest change in fracture toughness was observed in ZrC irradiated to a dose of 1.5 dpa, the increase is about 79%, however, it can also be found there are large measurement errors as the inherent uncertainty of the indentation fracture toughness measurement [27]. As explained by Clinard [28], the most appropriate irradiation toughening mechanism for ceramics is that involving the coherency strain field generated from a high density of Frank loops. A propagating crack would likely be deflected by the strain fields, resulting in crack impedance and consequent toughening.

4. Conclusion

The microstructure of proton irradiated ZrC at 800 °C to a dose of 0.7 and 1.5 dpa is primarily comprised of a high density of nanometer-sized Frank loops, with the average loop size around 5 nm

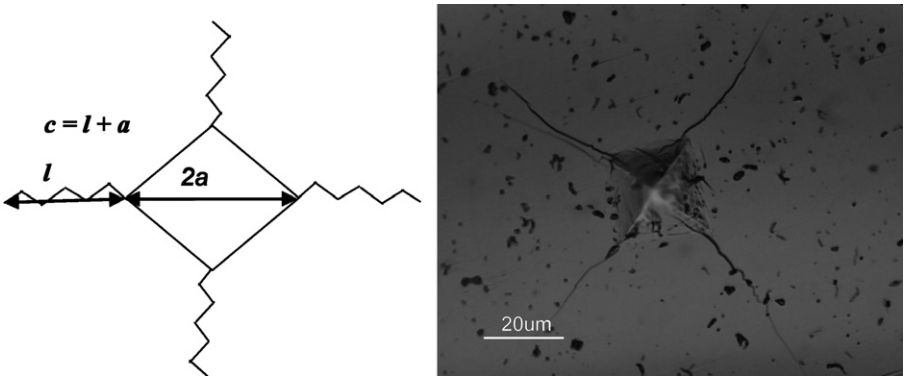

Fig. 12. Crack system developed in ZrC with Vicker indentation.

and the density increasing from $0.22 \times 10^{23}\,m^{-3}$ at a dose of 0.7 dpa to $3.37 \times 10^{23}\,m^{-3}$ at a dose of 1.5 dpa. No irradiation induced amorphization, voids or precipitates were observed. A slight lattice expansion was observed in the irradiated ZrC and the lattice expansion is in good agreement with the reported results from neutron irradiation studies. Regarding the mechanical property changes, increases were found for both the microhardness and fracture toughness of the irradiated samples, and the hardening behavior is likely related with high concentration of point defects.

Beyond this initial study, further investigations are needed to determine the nature of the small Franks loops, i.e. vacancy versus interstitial, Zr interstitial species versus C interstitial species, and to study the possible elemental depletion or enrichment using the EELS technique. Further research is also necessary to evaluate the influence of irradiation temperature on the microstructure evolution and the change of mechanical property.

Acknowledgement

This work is funded by the Department of Energy through Nuclear Energy Research Initiative program (Project 06-007 and Award #DE-FC07-06ID14740).

References

[1] C. Kral, W. Lengauer, D. Rafaja, P. Ettmayer, J. Alloy Compd. 265 (1998) 215.
[2] Y. Ozaki, R.H. Zee, Mater. Sci. Eng. A 202 (1995) 134.
[3] R. Evans, R. Jensen, M. Tishchenko, V. Daragan, AIP Conf. Proc. 301 (1994) 75.
[4] Gas-cooled Faster Reactor (GFR) FY04 Annual Report, INEEL/EXT-04-02361, 2004.
[5] K. Minato, T. Ogawa, K. Fukuda, H. Sekino, I. Kitagawa, N. Mita, J. Nucl. Mater. 249 (1997) 142.
[6] K. Sawa, S. Ueta, Nucl. Eng. Des. 233 (2004) 163.
[7] L.W. Hobbs, F.W. Clinard Jr., S.J. Zinkle, R.C. Ewing, J. Nucl. Mater. 216 (1994) 291.
[8] T. Ogawa, K. Fukuda, S. Kashimura, T. Tobita, F. Kobayashi, S. Kaod, H. Miyanishi, I. Takahashi, T. Kikuchi, J. Am. Ceram. Soc. 75 (1992) 2985.
[9] K. Minato, T. Ogawa, Global (2003) 1068.
[10] K. Minato, T. Ogawa, Kazuhiro Sawa, Nucl. Technol. 130 (2000) 272.
[11] M.S. Kovalchenko, Yu.I. Rogovoi, Neorg. Mater. 9 (1973) 321.
[12] R.A. Andrievskii, K.P. Vlasov, A.S. Shevchenko, A.G. Lantin, S.A. Pritchin, V.V. Klyushin, S.P. Krushin, A.S. Maskaev, Neorg. Mater. 14 (1978) 680.
[13] P. Patriarca, D.J. Rucker, Fuel and Materials Development Program Quarterly Progress Report for Period Ending September 30, 1969, ORNL-4480 1970.
[14] G.W. Keilholtz, R.E. Moore, M.F. Osborne, Nucl. Appl. 4 (1968) 330.
[15] J. Gan, M.K. Meyer, R.C. Birtcher, T.R. Allen, J. ASTM Int. 3 (2006) 1.
[16] D. Gosset, M. Dollé, D. Simeone, G. Baldinozzi, L. Thomé, J. Nucl. Mater. 373 (2008) 123.
[17] L.I. Gomozov, I. Sh. Akhmedzyanov, Soviet Atom. Energy 48 (1980) 413.
[18] Loo.F.J.J. Van, W. Wakelkamp, G.F. Bastin, R. Metselaar, Solid State Ionics, Diffusion & Reactions 32&33 (1989) 824. (pt. 2).
[19] R.A. Andrievskii, V.I. Savin, V. Ya Markin, V.T. Spravtsev, V.S. Shevshenko, Inorg. Mater. 14 (1978) 526.
[20] J.F. Ziegler, J.P. Biersack, U. Littmark, The Stopping and Range of Ions in Solids, Pergamon, New York, 1996.
[21] L. Van Brutzel, J.P. Crocombette, Nucl. Instr. and Meth. B 255 (2007) 141.
[22] S.J. Zinkle, in: 15th International Symposium on Effects of Radiation on Material, ASTM STP, n 1125, 1992, p. 749.
[23] Stoe & Cie, STOE WinXPOW (Version 1.06), Stoe & Cie GmbH, Darmstadt, Germany, 1999.
[24] ASTM standard: C 1327-03, Standard Test Method for Vickers Indentation Hardness of Advanced Ceramics.
[25] J.E. Sundgren, H.T.G. Hentzell, J. Vac. Sci. Technol. A 4 (1986) 2259.
[26] Evaluation of Alternate Materials for Coated Particle Fuels for the Gas-cooled Faster Reactor, Report, INL/EXT-06-11749, September, 2006.
[27] G.D. Quinn, J. Am. Ceram. Soc. 90 (2007) 673.
[28] F.W. Clinard Jr., G.F. Hurley, R.A. Youngman, L.W. Hobbs, J. Nucl. Mater. 133&134 (1985) 701.